VALIDATION OF PHOTOMETRICALLY CORRECTED LUNAR IMAGES. K. Macdonald, R. Lindsay, R. Procter-Murphy, A. Horchler, Astrobotic, 1016 N. Lincoln Ave, Pittsburgh, PA 15233 (research@astrobotic.com).

Introduction: Terrain Relative Navigation (TRN) is a mission critical capability that uses computer vision techniques to reduce spacecraft navigation uncertainty from the order of kilometers to the order of meters, enabling precision landing. Astrobotic's TRN solution requires a set of reference maps covering the range of potential trajectories, illumination conditions, and camera viewing angles to match the terrain features in camera images acquired during descent [1].

Satellite images of the lunar surface are publicly available from missions such as the Lunar Reconnaissance Orbiter (LRO) [2] and SELENE (Kaguya) [3]. Although over a million images are available, TRN requires large swaths of terrain at the precise illumination conditions prescribed by the mission. As such, it is necessary to extract surface features from the illumination effects induced by topography to enable subsequent rendering of target regions to predefined illumination conditions. In this abstract, the performance of several photometric models are evaluated to remove topographic shading from LRO Camera (LROC) Narrow Angle Camera (NAC) images.

Methodology: Surface reflectance at a specified wavelength is controlled by the geometric configuration of the scene, including the phase, incidence, and emission angles, seen in Figure 1.

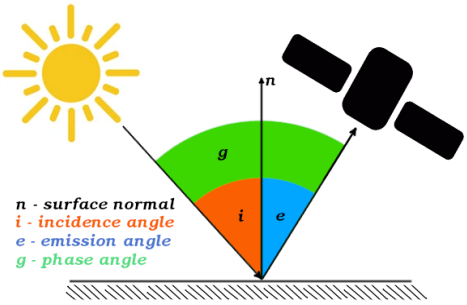

Figure 1. *Geometric angles based on spacecraft viewing angle, surface normal, and sun position.*

In this work, "reflectance" is defined as the radiance factor (I/F, unitless), or the reflectance relative to a perfect Lambertian surface observed and illuminated normally, as per [4]. Photometric models capture the dependence of reflectance on these angles, as well as on the particular scattering properties of the surface material. Three photometric models are considered: Lambert [5], Lunar Lambert [6], and Hapke [4]. Lambertian reflectance is based on the observation that surface brightness is dependent on the incidence angle, and is independent of the angles at which the surface is viewed. The Lunar Lambert model accounts for the dependence on viewing angle by employing the Lommel-Seeliger function at small phase angles, and Lambert's cosine law at large phase angles. This describes the multiple scattering among soil particles and macroscopic roughness more accurately than the Lommel-Seeliger function alone [7]. The spatial variation in the composition and maturity of the lunar regolith is accounted for by the Hapke model, which provides a set of empirically derived parameters to account for the physical properties of lunar regolith [8]. Each of these models is applied to the locally calculated phase, incidence, and emission angles to adjust the pixel brightness to a normalized viewing angle of (i, e, g) = (30°, 0°, 30°) [9].

Validation of the photometrically corrected data is critical to ensuring that 1) the dependence of reflectance on the angle of incidence is removed, and 2) shading artifacts are corrected such that data can be rendered to a date/time of interest. To address (2), the photometrically corrected image is rendered and compared to the illumination conditions of an independent target NAC image. This rendering is done using Astrobotic's LunaRay Suite [1], which employs physics-based ray tracing and SPICE-based ephemerides to simulate solar illumination on the terrain. The Structural Similarity (SSIM) index is used to quantify the similarity between the rendered and target NAC images [10], along with an average of the pixelwise root mean square error (RMSE).

Datasets: Results are presented for two regions: in Lacus Mortis southwest of Bürg crater (43.88N, 25.38E to 44.53N, 25.64E), and in the Highland Ponds region (42.35N, 167.42E to 42.95N, 167.93E). Lacus Mortis is the landing site for Astrobotic's Peregrine Mission 1. A wide range of geometric angles highlights the variations in the chosen photometric models, therefore a second more topographically varied area was chosen in the Highland Ponds region.

For the Lacus Mortis (LM) region, an internally generated and validated DEM at 4 m/pix was used. NAC image M110339496 was photometrically corrected and then rendered to the illumination conditions of M104354152. For the Highland Ponds (HP) region, a publicly available terrain model (HP 21 DTM) was used at 5 m/pix [11]. NAC image M1146059731 was photometrically corrected, rendered, and compared to M1183745548. The variations in incidence angles are outlined in Table 1, exemplifying a key topological difference between lunar maria and highlands.

Table 1. *Incidence angles for selected regions.*

Metric	LM	HP
Max/Min	77.35°/10.03°	98.55°/1.95°
Mean (Std. Dev.)	46.52° (4.52°)	50.42° (13.18°)

Results: Figure 2 compares the original NAC image to the Hapke photometric correction, along with the emission and incidence angle maps.

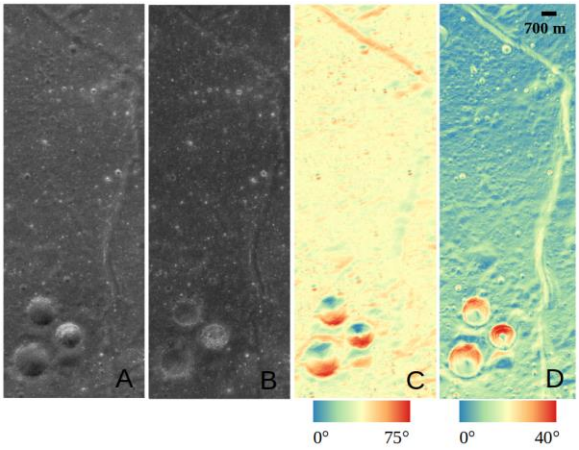

Figure 2. *A: NAC Image M110339496L. B: Corrected image. C: Incidence angles. D: Emission angles.*

A sample of rendered data to the illumination conditions of an independent image in the Highland Ponds region is shown in Figure 3.

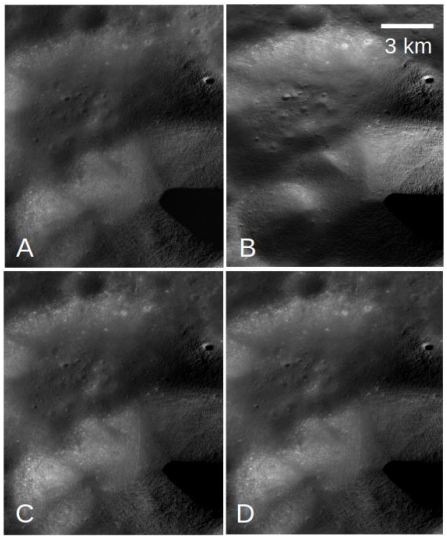

Figure 3. *A: NAC Image M1183745548. B: Lambert model correction. C: Lunar Lambert model correction. D: Hapke model correction.*

The dependence of reflectance on incidence angle can be understood by deriving the slopes of the line of best fit. Photometric correction effectively removes this coupling, as summarized in Table 2 for the two regions. Finally, in investigating the similarities between the rendered data and the target NAC image, SSIM was calculated to provide a similarity measure that accounts for luminance, contrast, and structure of either image. Additionally, the RMSE is calculated to show the average pixelwise difference between reference and rendered images. Table 3 summarizes these results.

Table 2. *Derived slopes between reflectance and incidence angle (units: reflectance per radian).*

Model	Slope LM	Slope HP
Original	-0.0259	-0.0519
Lambert	6.35E-5	-1.62E-4
Lunar Lambert	4.15E-5	9.66E-6
Hapke	2.74E-5	-2.21E-5

Table 3. *SSIM and RMSE results for corrected data.*

Model	SSIM LM	RMSE LM	SSIM HP	RMSE HP
Lambert	0.882	0.009	0.876	0.011
Lunar Lambert	0.952	0.006	0.966	0.005
Hapke	0.978	0.004	0.971	0.004

Producing accurate renderings to different illumination conditions was achieved by deriving the geometric angles of local topography and employing photometric models, thus removing topographic illumination effects in corrected images. The Hapke model consistently achieves the best results in similarity of renderings, and along with the Lunar Lambert model demonstrates a large increase in performance relative to the Lambert model alone. The Hapke model, however, is far more complex than the Lunar Lambert model, requiring the use of spatially varying parameters and more complex equations, impacting computation time. In practice, the tradeoff between complexity and output performance must be made depending on the application.

This effort progresses towards validating the use of this data for future missions employing TRN. Further work is required to derive the dependence of rendering accuracy on variation in image illumination conditions. These models of photometric correction have additionally been employed for SELENE Terrain Camera data. Work is currently underway to compare the derived reflectance values for these independent data sources, providing further opportunities for validation and a larger pool of data at varying extents and resolutions to aid in the production of mission relevant data.

Acknowledgments: This work has been supported by NASA Tipping Point 80LARC19C0008. NAC data was obtained via the Planetary Data System (PDS).

References: [1] Owens C. et al. (2021) *AIAA SciTech, 2021-0376.* [2] Robinson M. et al. (2010) *Space Sci. Rev., 150*, 81–124. [3] Kato M. et al. (2008) *Adv. Space Res., 42*, 294–300. [4] Hapke B. (2012) Theory of Reflectance and Emittance Spectroscopy, *CUP*. [5] Oren M. and Nayar S. (1995) *IJCV, 14*, 227–251. [6] McEwen A. (1991) *Icarus 92*, 298–311. [7] Yokota Y. et al. (2011) *Icarus, 215*, 639–660. [8] Sato H. et al. (2014) *JGR, 119*, 1775–1805. [9] McEwen A. (1996) *LPS XXVII*, 841-842. [10] Wang Z. et al. (2004) *IEEE Img. Proc., 13.* [11] Henriksen M. et al. (2017) *Icarus, 283*, 122–137.